Journal of Controlled Release 334 (2021) 11–20

Contents lists available at ScienceDirect

Journal of Controlled Release

journal homepage: www.elsevier.com/locate/jconrel

Sustained release of peptides and proteins from polymeric nanocarriers produced by inverse Flash NanoPrecipitation

Chester E. Markwalter [a,1], Robert F. Pagels [a,1], Ava N. Hejazi [b,2], Kurt D. Ristroph [a], Jiping Wang [b], Ke Chen [b], Jian Li [b], Robert K. Prud'homme [a,*]

[a] Dept of Chemical and Biological Engineering, Princeton University, Princeton, NJ, USA
[b] Biomedicine Discovery Institute, Infection & Immunity Program and Department of Microbiology, Monash University, Clayton, Melbourne, Victoria 3800, Australia

ARTICLE INFO

Keywords:
Nanocarriers
Nanoparticles
Biologics
Antibiotics
Sustained release
Pulmonary delivery

ABSTRACT

Peptide and protein therapeutics generally exhibit high potency and specificity and are increasingly important segments of the pharmaceutical market. However, their clinical applications are limited by rapid clearance and poor membrane permeability. Encapsulation of the peptide or protein into a nano-scale carrier can modify its pharmacokinetics and biodistribution. This might be employed to promote uptake in desired cell types or tissues, to limit systemic exposure, or to reduce the need for frequent injections. We have recently described inverse Flash NanoPrecipitation (iFNP), a scalable technique to encapsulate water-soluble therapeutics into polymeric nanocarriers, and have demonstrated improvements in therapeutic loading of an order of magnitude over comparable approaches. Here, we describe the formulation parameters that control release rates of encapsulated model therapeutics polymyxin B, lysozyme, and bovine serum albumin from nanocarriers produced using iFNP. Using a neutropenic lung infection mouse model with a multi-drug resistant *Acinetobacter baumannii* clinical isolate, we demonstrate enhanced therapeutic effect and safety profile afforded by nanocarrier-encapsulated polymyxin B following pulmonary administration. The encapsulated formulation reduced toxicity observed at elevated doses and resulted in up to 2.7-$\log_{10}$ reduction in bacterial burden below that of unencapsulated polymyxin B. These results establish the promise of iFNP as a platform for nanocarrier delivery of water-soluble therapeutics.

1. Introduction

There are no marketed nano-scale delivery vehicles for oligopeptides and proteins, even though such constructs have been explored extensively for 50 years [1–3]. By contrast, there are several approved nano-scale formulations for hydrophobic drugs and for RNA therapeutics, such as Doxil and Onpattro, respectively [4,5]. Encapsulation of peptides and proteins continues to garner interest because of the potential to overcome limitations in cell uptake, protease degradation, and renal filtration. A nanocarrier (NC) formulation can impart this functionality without compromising the specificity and potency that characterizes this class of therapeutics [3,6–8].

The primary barriers hindering existing formulation methods, exemplified by liposomes and polymersomes, are low loading (weight fraction therapeutic) and poor encapsulation efficiency (fraction of therapeutic successfully captured within the nanocarrier) [1,7]. Typical loadings in the 1–5 wt% range mean that the vast majority of the injected material is excipient [9]. To address this, we developed a solubility-driven sequential assembly process called inverse Flash NanoPrecipitation (iFNP) that produces highly loaded polymeric NCs using scalable processing steps [10,11]. The method produces water-dispersed NCs 50–200 nm in diameter with the encapsulated therapeutic located in a hydrophilic core surrounded by a hydrophobic polymer shell. The nanoparticle is stabilized by an external hydrophilic polymer brush (Fig. 1A). While the shell is analogous to a polymersome, the core is comprised of the therapeutic rather than the aqueous environment of liposomes and polymersomes.

The iFNP process produces an "inverse nanocarrier" by rapid mixing of a stream containing the therapeutic and a block copolymer such as poly(aspartic acid)-*b*-poly(lactic acid) (PAsp-*b*-PLA) with a lipophilic

* Corresponding author at: A301 Engineering Quad, Olden St, Princeton, NJ 08544, USA.
E-mail address: prudhomm@princeton.edu (R.K. Prud'homme).
[1] Optimeos Life Sciences, 174 Nassau St Princeton NJ, USA.
[2] University of California, Berkeley, Berkeley, CA, USA.

https://doi.org/10.1016/j.jconrel.2021.04.002
Received 25 January 2021; Received in revised form 31 March 2021; Accepted 2 April 2021
Available online 3 April 2021

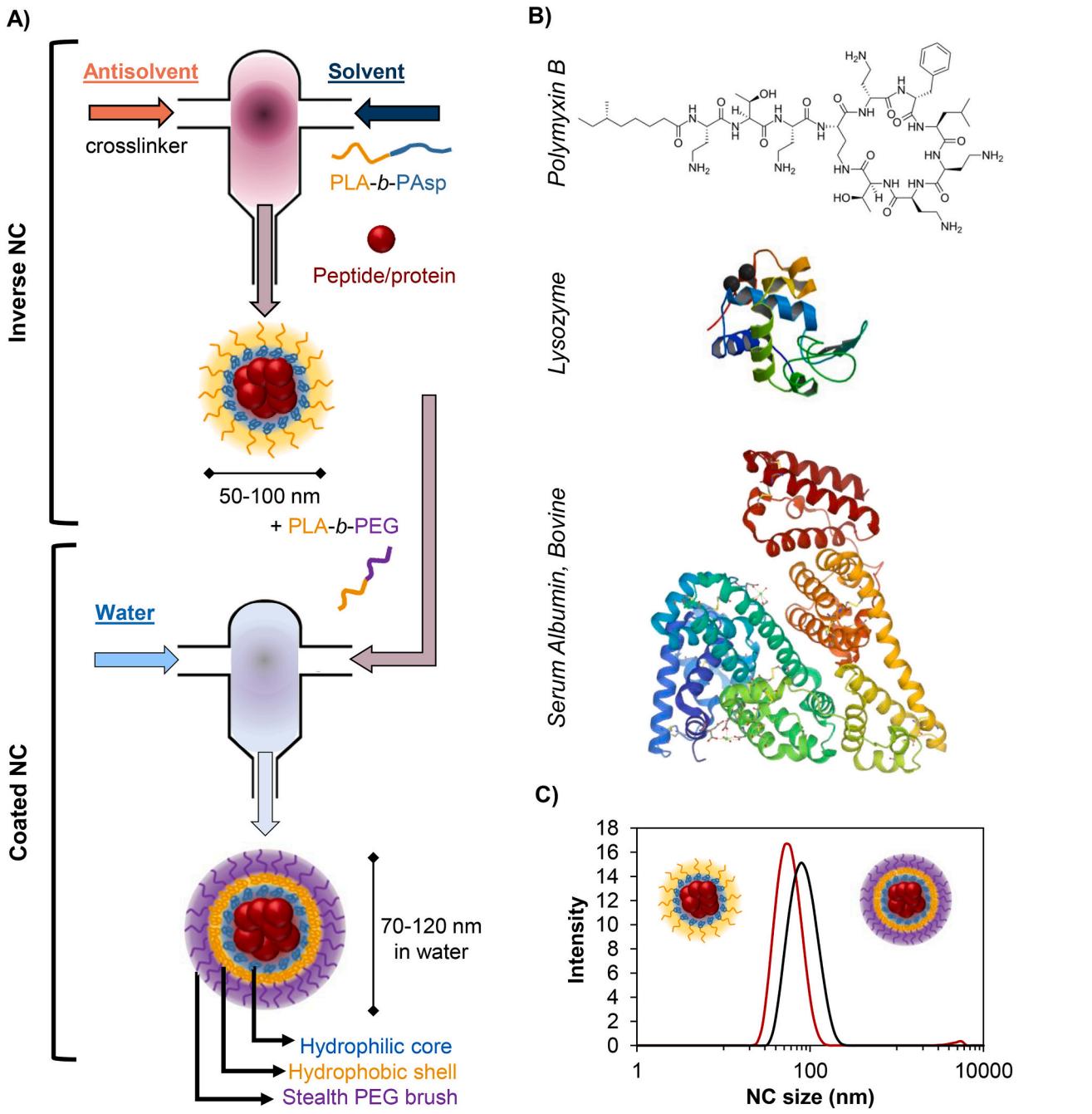

Fig. 1. (A) Inverse Flash NanoPrecipitation (iFNP) process schematic showing the assembly of the inverse nanocarrier (NC) and the PEG coating step. (B) Structures of models polymyxin B, lysozyme (Lys), and bovine serum albumin (BSA) employed in this work. Protein structures are from the Protein Databank (Lys- 1DPX, BSA – 4F5S). (C) Dynamic light scattering analysis of standard polymyxin B formulation with the inverse NC trace (red) and the PEG-coated NC trace (black). (For interpretation of the references to colour in this figure legend, the reader is referred to the web version of this article.)

solvent (*e.g.* dichloromethane). Typical mixers that can achieve high volumetric flowrates and rapid mixing are a confined impinging jet (CIJ) mixer and a multi-inlet vortex mixer (MIVM) [12–14]. The inverse nanocarrier is dispersed in the lipophilic solvent, sterically stabilized by the PLA shell. The core contains the therapeutic as a precipitated solid, since it is not soluble in the external lipophilic solvent. It is often desirable to stabilize the inner PAsp layer by introducing a multivalent cation such as Ca^{+2}, Zn^{+2}, or a polyamine such as tetraethylenepentamine (TEPA), which interacts with the PAsp core to produce a hydrogel-like structure [10,15]. The details of the processing steps have been described previously [10]. These inverse NCs are made water-dispersible through the assembly of a biocompatible block copolymer on the NC surface by a second Flash NanoPrecipitation step using aqueous media. The second amphiphilic stabilizing polymer is typically polylactic acid-*b*-poly(ethylene glycol) (PLA-*b*-PEG).

These sequential process steps produce NCs with near-neutral zeta potentials and narrow size distributions [10]. The initial installation of a PLA shell in a lipophilic solvent limits therapeutic escape upon exposure to aqueous environments, enabling exceptionally high loading values. We have encapsulated peptides, proteins, and oligonucleotides at therapeutic loadings as high as 27 wt% [10]. Those steps in the process that affect the release kinetics of the active are explored below.

The architecture produced by iFNP, consisting of a crosslinked hydrophilic core contained within a thin hydrophobic shell, suggests

several mechanisms that may contribute to the control of therapeutic release kinetics. NCs with a complete PLA shell are expected to release encapsulated material by hydrolytic degradation of the PLA. This would be analogous to the release behavior observed for degradable polymersomes, where pore formation occurs as hydrolysis proceeds [16,17]. For the iFNP system, we anticipate that pore formation would be more rapid than hydrolytic degradation alone because the T_g of the PLA shell is near physiological temperature, permitting accelerated shell rearrangement [18,19]. A second mechanism influencing release is ion exchange from the buffer, which is expected to destabilize the crosslinked polyanionic core (*i.e.* PAsp/Ca).

Herein, we report design rules to establish sustained release of model proteins lysozyme (Lys) and bovine serum albumin (BSA), as well as a therapeutic peptide, polymyxin B (PmxB), from these NCs (Fig. 1B). We sought formulations that impart a sustained release profile of the encapsulated therapeutic under physiological conditions while minimizing rapid burst release within the first 15 min. We formulated PmxB, Lys, and BSA into coated NCs (Fig. 1C) and evaluated the effect of formulation parameters on release. We assessed several polymer architectures: a first generation ("Gen1") $PAsp_{5kDa}$-*b*-PLA_x-*b*-$PAsp_{5kDa}$ with varied PLA block size ("x") and a second generation ("Gen2") $PAsp_{2kDa}$-*b*-PLA_{15kDa}. We also varied the crosslinker type (TEPA, calcium, and zinc) in selected formulations. Finally, we assessed the effect of the lactide:glycolide ratio by replacing PLA with a 50:50 poly(lactic-*co*-glycolic) acid (PLGA) block in the Gen2 polymer. In all cases, the inverse NC was coated with $PLA_{4.2k}$-*b*-$mPEG_{5k}$. We found that the polymer architecture (as well as the encapsulated material itself) dictated release behavior. We then employed PmxB formulated by iFNP in a murine gram-negative lung infection model to demonstrate the clinical efficacy and enhanced safety profile of the sustained release formulation.

2. Materials and methods

2.1. Materials

TWEEN® 20 (BioXtra), tetraethylenepentamine (technical grade), calcium nitrate tetrahydrate (99%, ACS grade), Boc-glycine (≥99.0%), N-(3-dimethylaminopropyl)-N′-ethylcarbodiimide hydrochloride (EDC, ≥98.0%), 4-(dimethylamino)pyridine (DMAP, prilled, 99%), triethylamine (TEA, 99%), bovine serum albumin (fatty acid free, low endotoxin, >96%), and lysozyme from chicken egg white (>90%) were purchased from Sigma-Aldrich (St. Louis, MO). Sodium chloride (ACS grade), Pierce BCA Protein Assay Kit, AlexaFluor-488 5-SDP ester, acetone (ACS grade), dimethyl sulfoxide (HPLC grade), methanol (HPLC grade), chloroform (ACS grade), methylene chloride (ACS grade), and tetrahydrofuran (HPLC grade) were purchased from Thermo Fisher Scientific (Waltham, MA). Isopropyl alcohol, toluene, and hexanes were all of ACS grade and purchased from Fisher Scientific (Hampton, New Hampshire). Trifluoroacetic acid (peptide synthesis grade), diethyl ether (anhydrous, HPLC grade), absolute ethanol, chloroform (extra dry, over sieves), and dichloromethane (extra dry, over sieves) were also purchased from Fisher Scientific (Hampton, New Hampshire). Hydrogen bromide (pure, 33 wt% solution in glacial acetic acid) was purchased from Acros Organics. β-Benzyl L-aspartic acid N-carboxyanhydride (Benzyl-Asp-NCA) was purchased from Toronto Research Chemicals Inc. Ester-terminated poly(DL-lactic acid) (Resomer R203 S) and poly(lactic acid-*co*-glycolic acid) (Resomer RG 503) were provided by Evonik (Essen, Germany). $PLA_{4.2k}$-*b*-$mPEG_{5k}$ was a gift from Evonik (Essen, Germany). Sodium azide was purchased from Eastman Chemical (Kingsport, TN). Ammonium hydroxide 28–30% solution in water (ACS grade) was purchased from Acros Organics (Waltham, MA). Polymyxin B sulfate was purchased from Calbiochem (St. Louis, MO). Bio-Whittaker® phosphate-buffered saline (without calcium or magnesium) was purchased from Lonza (Basel, Switzerland). Deionized water (MQ) (18.2 MΩ·cm) was generated by a NANOpure Diamond UV ultrapure water system (Barnstead International, Germany).

Triethylamine (TEA) was distilled at atmospheric pressure under nitrogen. 4-(dimethylamino)pyridine (DMAP) was recrystallized three times from toluene and dried under high vacuum before use. All other materials were used as received.

Polymyxin B and its nanoparticle formulations were stored at −80 °C until freshly prepared in sterile Milli-Q water [20]. A multi-drug resistant clinical bacterial isolate *A. baumannii* FADDI-AB051 (0.5 mg/L) was employed and subcultured prior to the experiment [21,22]. Minimum inhibitory concentrations were determined using the broth microdilution method in cation-adjusted Mueller-Hinton broth (CAMHB) [23] without polysorbate 80 or mucin.

2.2. Protein labeling with Alexa Fluor 488

Lysozyme (Lys) or bovine serum albumin (BSA) was dissolved in a bicarbonate buffer (pH 8.2, 0.15 M) at 20 mg/mL. Alexa Fluor 488 5-SDP ester was dissolved in DMSO at 10 mg/mL and 0.15 eq was added to the protein solution with mixing. The reaction proceeded at room temperature for 2 h, protected from light. The reaction mixture was rinsed on 3 kDa Amicon ultrafilters (Amicon Ultra-2, MilliporeSigma) by centrifugation at 5000 RCF with PBS buffer (4 volumes) followed by deionized water (4 volumes). The protein was recovered and lyophilized. A single fluorescent band corresponding to Lys was observed by SDS-PAGE.

2.3. Poly(aspartic acid)-b-poly(lactic acid) synthesis

The Gen1 $PAsp_{5k}$-*b*-PLA_x-*b*-$PAsp_{5k}$ was synthesized as described previously [10]. The Gen2 $PAsp_{2k}$-*b*-PLA_{15k} and $PAsp_{2k}$-*b*-$PLGA_{15k}$ were prepared using PLA or PLGA, respectively, as a macroinitiator. The starting PLA was Resomer R203 S (Evonik) which had an M_n of 9200 Da by ^{1}H NMR. The starting PLGA was Resomer RG503 (Evonik), which was composed of 50% glycolic acid and 50% lactic acid, and had an M_n of 15,000 Da by ^{1}H NMR. Both the PLA and PLGA had one ester-terminated end and one hydroxyl-terminated end.

The hydroxyl end groups of the PLA and PLGA were converted to amines through two synthetic steps. First, the carboxylic acid of Boc-glycine was conjugated to the hydroxyl end group of the PLA or PLGA by a Steglich esterification. The polymers (10 g) were dried from toluene by distillation three times (note: the PLGA did not fully dissolve in toluene), followed by drying under high vacuum. Boc-glycine (2.5 eq), N-(3-dimethylaminopropyl)-N′-ethylcarbodiimide hydrochloride (EDC, 2.5 eq), and 4-(dimethylamino)pyridine (DMAP) (2.5 eq) were added to the polymer flask and dried under high vacuum. The flask was purged with argon, and dry $CHCl_3$ was added to produce a 20 mM polymer solution. The reaction proceeded for 72 h, after which the solution was washed with ice-cold 0.1 M HCl three times to remove the EDC and DMAP, followed by three washes with ice-cold water. The polymer was then precipitated into cold IPA (0 °C) three times to remove the excess Boc-glycine and dried under high vacuum overnight. Next, the Boc protecting group was removed using trifluoroacetic acid (TFA). The polymers were first dried from toluene by distillation three times and then dissolved in dry DCM followed by the addition of TFA to produce a 15 v% TFA solution with a 10 mM concentration of Boc groups. The deprotection occurred over 4 h, after which the polymer was precipitated into dry ice-cold diethyl ether. The resulting polymer was dissolved in DCM with 10 equivalents of triethylamine (TEA) added to generate the free base of the amine-terminate polymer. The polymer/TEA solution was mixed for 30 min, then was precipitated into ice-cold IPA two times before being precipitated into hexanes. The polymer was dried under high vacuum overnight.

The amine-terminated polymers were used as macroinitiators for the ring-opening polymerization of the benzyl-Asp-NCA monomer. The macroinitiators (1 eq. of amine groups) were dried from toluene by distillation three times, followed by drying under high vacuum for 3 h. The benzyl-Asp-NCA monomer (17.4 eq, targeting a 2 kDa PAsp block)

was added to the macroinitiator flask and dried under high vacuum. The flask was purged with argon, and dry $CHCl_3$ was added to produce a 5 mM solution of amine end groups. The solution was warmed to 40 °C for 24 h under argon balloon. After 24 h, an equal volume of 33 wt% HBr in acetic acid was added to the solution to deprotect the PAsp side groups. After 1 h, the polymers were precipitated in ice-cold diethyl ether three times, twice in IPA and a final wash with hexanes. The polymer was dried under high vacuum overnight. Prior to use, the PLGA-*b*-PAsp and PLA-*b*-Asp block copolymers were dissolved in DMSO at a concentration of 100 mg/mL and placed inside dialysis tubing with a 6–8 kDa molecular weight cutoff. The dialysis tubing was placed in a large stirring water bath, and the polymer was dialyzed at room temperature for 2 h, and at 4 °C for 24 h, with four changes of the water bath. The purified polymer was lyophilized and stored at −20 °C.

2.4. NC fabrication

Inverse NCs were prepared as previously described [10]. In short, the polymer stabilizer and the peptide or protein were combined in DMSO at the desired ratio at a total concentration of 5–15 mg/mL. Inverse NCs were prepared in a confined impinging jet (CIJ) mixer with chloroform (Lys and BSA) or dichloromethane (PmxB). Calcium crosslinking was carried out using a 1:1 charge ratio with respect to total Asp residues. This component was first dissolved in methanol, and the solution was included in the antisolvent stream at 10 vol%. 0.6 equivalents of ammonia, diluted in methanol, was added dropwise (50 μL) to the inverse NC dispersion after formation. For Lys formulations, except where indicated, tetraethylenepentamine (TEPA) was used at 0.6 equivalents and was added dropwise after inverse NC formation in lieu of calcium and ammonia. The 5 k blue dextran formulation was prepared as described in our previous publication [10].

The crosslinking proceeded for 30 min. (The BSA formulation was stored overnight cold before proceeding.) Excess crosslinker and DMSO were removed in a 30-min extraction, where the aqueous phase contained 150 mM sodium chloride. The inverse NC dispersion was retained in the organic phase, which was isolated and then solvent exchanged by rotary evaporation into tetrahydrofuran (THF) or acetone. $PLA_{4.2k}$-*b*-PEG_{5k} was added at a desired mass ratio relative to the inverse NC (varying from 0.5:1 to 0.75:1), assuming complete encapsulation efficiency to calculate the inverse NC mass. This stream was concentrated to around 7.5–15 mg/mL inverse NC, determined by volume measurement of the dispersion after solvent exchange. The PLA-*b*-PEG coating was installed by rapid mixing against an equal volume of water in a CIJ. An additional dilution of water was included in the collection vessel to ensure that the organic solvent represented no more than 10 vol% of the dispersion. The BSA formulation contained 150 mM NaCl in the water.

Loading and other key parameters are summarized in Table 1. A theoretical (target) loading for the coated NC was calculated as:

$$Loading = \frac{[encapsulant]}{[encapsulant] + [polymer_1] + [polymer_2]} * 100$$

$Polymer_1$ represents the amount of stabilizer used for the inverse NC step. $Polymer_2$ corresponds to the stabilizer used during PEG coating. Polymer abbreviations used herein are as follows: $PAsp_{5k}$-*b*-PLA_x-*b*-$PAsp_{5k}$ is listed as Gen1-(x/2) where the PLA molecular weight is divided in half to reflect the "folded over" nature of triblock assembly. The second-generation polymers, $PAsp_{2k}$-*b*-PLA_{15k} and $PAsp_{2k}$-*b*-$PLGA_{15k}$, will be listed as Gen2-PLA and Gen2-PLGA respectively. The PLGA contained a 50:50 lactide to glycolide ratio.

Table 1
Formulation summary for coated NCs produced by iFNP. The inner polymer refers to the stabilizer used in forming the initial inverse NC. $PLA_{4.2k}$-*b*-PEG_{5k} was used in the coating step in all cases.

ID	Encapsulant	Inner polymer	Target NC loading	Crosslinker
1	Lys	Gen1-20	19%	TEPA
2	PmxB	Gen1-5	33%	Ca^{2+}
3	PmxB	Gen1-20	17%	Ca^{2+}
4	Lys	Gen2-PLA	13%	TEPA
5	PmxB	Gen2-PLA	14%	Ca^{2+}
6	Lys	Gen2-PLA	13%	Ca^{2+}
7	PmxB	Gen2-PLGA	14%	Ca^{2+}
8	BSA	Gen2-PLA	15%	Ca^{2+}

2.5. NC purification for release studies

Coated NCs were concentrated on 100 kDa Amicon ultrafilters (Millipore-Sigma, St Louis, MO) to around 200 μL. The filter permeate was weighed and lyophilized. The residue was later redissolved in release buffer and analyzed for losses. Approximately 2 mL of deionized water was added to the NC dispersion on the ultrafilter and again concentrated. This was repeated a second time to generate a purified NC dispersion in water. (For BSA formulations, the water washes contained 150 mM NaCl.) The wash permeates were weighed, pooled, and lyophilized as above. Release buffer was later added to the dried permeate residue and analyzed for losses. The release buffer was 1× phosphate buffered saline (PBS) buffer with 0.02 wt% sodium azide added as a preservative and TWEEN® 20 at 0.02 wt% as a hydrophobic component. The purified NC dispersion was diluted into release buffer at a target encapsulant concentration of around 0.15–0.3 mg/mL. This ultrafiltration process removed organic solvent and unencapsulated peptide or protein.

Encapsulation efficiency (EE) was calculated from the ultrafilter permeate as follows (after confirming there were minimal losses to the ultrafilter under filtration conditions):

$$EE = \left(1 - \frac{[encapsulant\ in\ permeate\ solution]}{[encapsulant\ added]}\right) \times 100$$

2.6. Release protocol

After ultrafiltration purification, the concentrated NC dispersion was diluted into release media. The dispersions were then tightly sealed and incubated at 37 °C in an orbital shaker. Low level adsorption to the glass of the vial was countered *via* prewashing with PBS containing 0.02 wt% TWEEN® 20. Controls of soluble Lys in buffer indicated that no fluorescence loss was observed over time. At each indicated time point, the dispersion was thoroughly mixed and a sample was removed. The sample was characterized for size (DLS), surface charge (zeta potential), and extent of release.

To measure extent of release, the NC dispersion (250 μL) was added to a 100 kDa Amicon ultrafilter (or 300 kDa Pall NanoSep for BSA). Each filter had previously been washed with a 0.5 mg/mL solution of unlabeled Lys (for Lys formulations) or PBS with 0.02 wt% TWEEN® 20 buffer (PmxB and BSA formulations). This removed preservative from the filter and reduced nonspecific binding. Controls indicated complete recovery of soluble analyte in the permeate using these pre-wash conditions. After ultrafiltration to concentrate the NC dispersion to 50 μL or less, 250 μL of fresh release media was added to the dispersion and concentrated again. The combined permeate was then analyzed for released encapsulant according to the methods detailed below. The retentate was resuspended in a defined volume and recovered for analysis of residual encapsulant in the NCs (SI Fig. S-1). Since all free encapsulant was removed during the initial ultrafiltration purification of the NCs, the release curves inherently begin at 0% release and include a data point to reflect this. For all release curves, a sample was taken immediately after dilution into release buffer (before heating to 37 °C) to measure a "burst release" value. It is plotted in the figures at 0.25 h.

2.7. Concentration measurements

Lys or BSA fluorescence was measured ($\lambda_{ex} = 490$ nm, $\lambda_{em} = 520$ nm)

using a SpectraMax i3x plate reader (Molecular Devices) to determine concentration in the ultrafilter washes and the release samples. The filter retentate fluorescence was also measured to determine the content retained in the NC core, but total concentration corrections were only used at long times when the retentate content was less than 10% to avoid fluorescence quenching. For BSA, the standard bicinchoninic acid (BCA) assay was used to quantify total protein at the start of release and was found to be in good agreement with the filter permeate loss measurements.

PmxB concentration was measured by HPLC using a Waters XSelect HSS T3 column (3.5 μm). A water/acetonitrile/trifluoracetic acid gradient elution was used as previously reported at 1 mL/min and 27 °C, with detection at 220 nm [10]. Concentrations were determined by summation of all peaks present in the initial material between 5.5 min and 6.2 min. The total content in the retentate was measured using the standard bicinchoninic acid (BCA) assay of the NC dispersion, which were incubated for 1 h at 37 °C. We have found that this incubation degrades the PLA shell and allows full quantitation of the encapsulated PmxB in agreement with HPLC analyses.

2.8. Lyophilization study

After completing the water rinses of the coated NC dispersion by ultrafiltration, we added approximately 1 mL of a solution containing 5 wt% trehalose and 5 wt% (2-hydroxypropyl)-β-cyclodextrin (HPβCD) for every 2.5 mg of PmxB used in the formulation. We recovered the NC dispersion from the filter using the manufacturer's method of inverting the ultrafilter device. Additional 0.25 mL of the saccharide solution was added to the filter and any remaining NC was resuspended by vigorous pipetting. This suspension was recovered using the inversion protocol a second time and combined with the first sample. The dispersion was then rapidly frozen with acetone chilled using dry ice. After lyophilization, the NCs were dispersed by the addition of deionized water (equal volume to the lyophilized solution). This dispersion was concentrated on an ultrafilter and rinsed once with DI water to remove excess cryoprotectant. These washes were pooled to evaluate loss of encapsulant in this step. The NC dispersion was then diluted in release media and monitored as before.

2.9. Neutropenic murine lung infection model

Animal experiments were approved by the Monash University Animal Ethics Committee (MARP-2) and animals were maintained in accordance with the criteria of the Australian Code of Practice for the Care and Use of Animals for Scientific Purposes. Female Swiss mice (8 weeks old, 25–30 g body weight) were obtained from Monash Animal Services (Clayton, Victoria, Australia) and were rendered neutropenic by cyclophosphamide [20–22]. Mice were anaesthetized by inhaled isoflurane and rested in the supine position against a restraining board. Each mouse was inoculated with 25 μL of bacterial suspension in saline ($\sim 10^5$ *A. baumannii* bacterial cells in early logarithmic growth phase) sprayed directly into the trachea using a MicroSprayer® Aerosolizer (model IA-1C; Penn-Century, Philadelphia, PA, USA).

Subsequently, mice were held upright on the restraining board for 2 min and then placed on a warm pad for recovery from anaesthesia. Polymyxin treatment (intratracheal spray of PmxB and its NC formulations at a single dose of 5 mg/kg or 10 mg/kg) was initiated 2 h following inoculation ($n = 3$). Bacterial loads in the lungs were determined in untreated control and polymyxin-treated mice at 2 h after inoculation (untreated controls) and 24 h after polymyxin treatment [20–22]. Statistical analysis was conducted with JASP open-source software using a one-way ANOVA followed by *post hoc* test corrected with Tukey HSD for multiple comparisons (significant p-value <0.05).

3. Results and discussion

3.1. Rapid release from NCs produced with Gen1 polymer stabilizers

Inverse NCs containing PmxB or Lys were formed using the Gen1 polymer stabilizer of varying PLA block size. For all formulations, the same PLA-*b*-PEG polymer stabilizer was used to install the outer layer. This allowed an assessment of the effects of crosslinking and PLA block size on release rate. The NCs were produced using the standard process described previously [10]. The sequential assembly steps afforded coated NCs with high loadings (Table 2). For all tested formulations, we maintained a constant mass ratio between the PAsp block and the model therapeutic. Therefore, the target loading changed in tandem with the relative block sizes of PLA. The encapsulation efficiency for Lys was 90–97% and for PmxB was 70–80% across the different formulations. As noted below, formulations exhibited minimal release or size change in DI water for 24 h.

We monitored release from the coated NCs at 37 °C in isotonic PBS supplemented with 0.02 wt% TWEEN® 20. Release was initiated by diluting a concentrated aqueous NC dispersion into the media to a concentration no greater than 0.3 mg/mL encapsulant. An initial time point was sampled after dilution but before heating to 37 °C. This will be referenced as the "burst release" fraction and is plotted at time 0.25 h for all curves. This value represents near-instantaneous release of NC-associated peptide or protein because unencapsulated material was removed by extensive aqueous washes prior to media exposure.

Release of PmxB from Gen1 NCs exhibited rapid 80% burst followed by a transition to a slow release phase, which continued over about 24 h (Fig. 2A). There was no effect from a 4-fold increase in PLA molecular weight. By contrast, Lys release exhibited a reduced burst (55%) but complete release was observed by the first time point taken at 37 °C (SI Fig. S-2). Such rapid profiles indicate that release is not dependent upon hydrolytic degradation of PLA, which occurs over weeks to months [24–26]. We hypothesized that salts in the release media rapidly acted to disrupt favorable ionic interactions between the negatively charged PAsp and the positively charged PmxB or Lys. The same process also results in disruption of the calcium crosslinking stabilizing the core. Indeed, Lys NCs diluted into sucrose solution exhibited minimal release until the addition of 150 mM NaCl to the dispersion, at which point the rapid Lys profile was recapitulated (SI Fig. S-3). This demonstrates that the ion-exchange process, rather than the temperature shift from

Table 2
Characterization of NCs produced by the iFNP process (average ± SD of triplicate samples). Gen1 formulations have been previously reported and characterized [10].

ID	Encapsulant	Inner polymer	Coated NC size (nm)	ζ (mV)	PDI	Actual loading (wt %)
1	Lys	Gen1-20	140 ± 19	NT	0.29 ± 0.04	19
2	PmxB	Gen1-5	131 ± 3	NT	0.10 ± 0.01	27
3	PmxB	Gen1-20	119 ± 7	−2.1 ± 0.7	0.13 ± 0.01	16
4	Lys	Gen2-PLA	69 ± 4	−4.2 ± 0.5	0.18 ± 0.01	13
5	PmxB	Gen2-PLA	100 ± 1	−1.4 ± 0.2	0.15 ± 0.01	10
6	Lys	Gen2-PLA	94 ± 22	−5.7 ± 0.7	0.22 ± 0.04	13
7	PmxB	Gen2-PLGA	87 ± 5	−1.5 ± 0.2	0.11 ± 0.01	10
8	BSA	Gen2-PLA	68 ± 4	−9.6 ± 0.3	0.27 ± 0.04	11

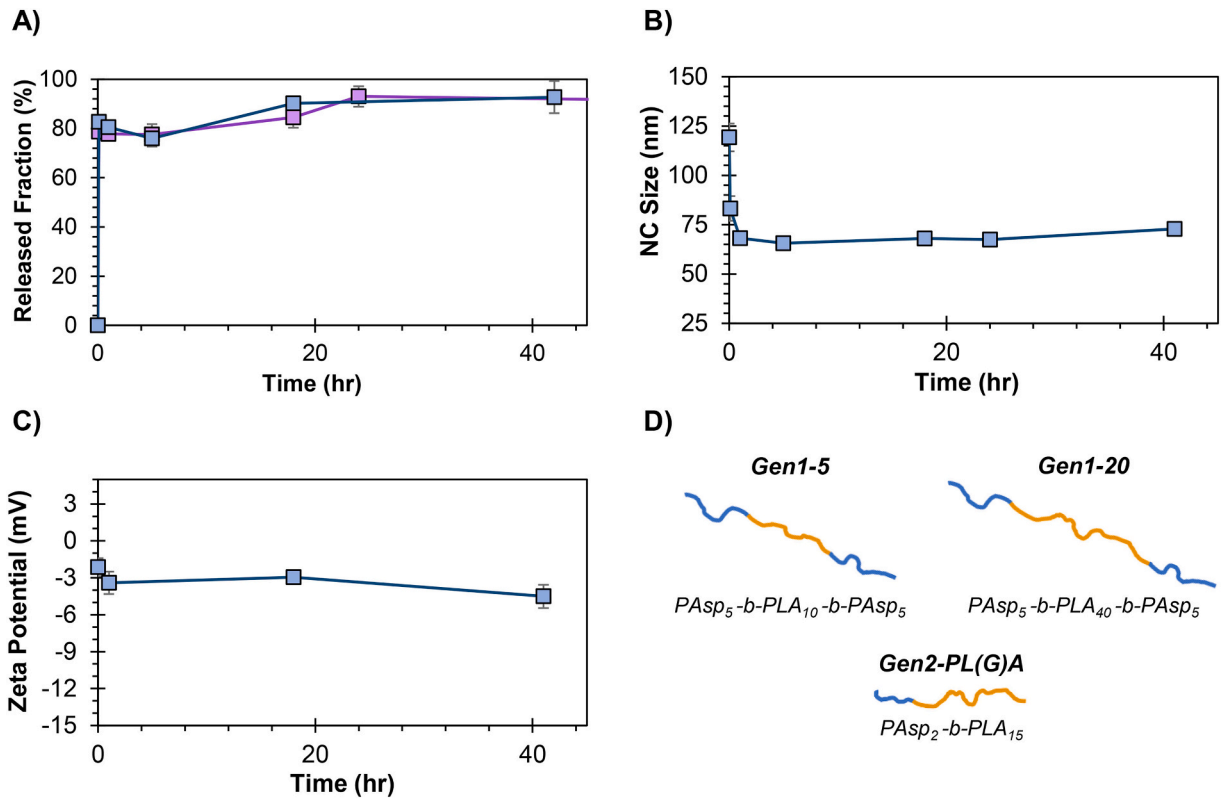

Fig. 2. (A) *In vitro* release profile of PmxB from Gen1 polymer stabilizers (purple: Gen1-5, blue: Gen1-20. Formulation ID-2 and ID-3 from Table 1, respectively). (B) NC size change by DLS for PmxB formulation ID-3 (Gen1-20 polymer stabilizer) monitored during release. (C) Zeta potential measurements of the same. The zeta potential was measured in 0.1× PBS. (D) Schematics of Gen1 and Gen2 block copolymer structure. Naming convention for Gen1 polymers used half of the PLA molecular weight to reflect the actual PLA brush height after nanocarrier assembly. (For interpretation of the references to colour in this figure legend, the reader is referred to the web version of this article.)

ambient to 37 °C is the dominant mechanism behind the observed burst release.

The size and zeta potential were also monitored during release. Representative data are shown in Fig. 2B and C. For all formulations, NC size shrunk rapidly followed by stabilization at significantly smaller size (~60 nm). The zeta potential, however, remained largely neutral over the time course. This reduction in size was enabled because the T_g of the PLA stabilizer, when hydrated, is at or below the release temperature [18,19]. By contrast, incubation at 20 °C resulted in slower rate of size change and coincided with slowed release kinetics at lower temperatures (SI Figs. S-4 and S-5).

The behavior of NCs formed with Gen1 polymers may best be understood as the balance of osmotic forces and restraining elastic forces. The core possesses a high osmotic pressure from the high concentration of Lys or PmxB. The osmotic pressure of Lys solutions has been studied by McCarty et al. [27] and Moon et al. [28] but at much lower protein concentrations than are present in our NC cores. The encapsulating shell is composed of the dense PAsp corona that is crosslinked by both Ca^{+2} and the cationic lysozyme or PmxB. Once exposed to a 150 mM ionic solution, ion exchange eliminates some fraction of the ionic bonds holding the shell together. The result is a weakening, but not elimination, of the shell and immediate release of a substantial fraction of the core (80% release for Gen1 block copolymer). While the crosslinked internal corona contributes to the stability of the NC prior to ion exchange, the PLA bilayer shell also plays an important role as ion exchange progresses. The observed reduction in kinetics of release and shell rearrangement at lower temperatures suggests the PLA dynamics are required for release of core material. The size reduction also results in reduced surface area per mass of PLA around the core, leading to a more robust PLA shell. This coincides with the secondary, slower phase of release. Release in this second phase may proceed by the poration mechanism postulated by the Discher group for polymersome release [17]. There is an excess of negative charge (PAsp residues) relative to the positive charge on PmxB or Lys in the NC formation, further supporting that this rate transition reflects shell effects rather than charge equilibrium acting to retain the encapsulated compound. These observations are in excellent agreement with our previous report, where we hypothesized that the relative PAsp and PLA block sizes could contribute to an incomplete PLA shell [10]. We therefore produced a second generation (Gen2) diblock copolymer stabilizer that contained a smaller PAsp block and a PL(G)A block size similar to the largest Gen1 stabilizer we had tested (Fig. 2D).

3.2. Gen2 polymer stabilizers reduce burst and produce sustained release profiles

We formulated PmxB, Lys, and BSA with Gen2 polymers and then evaluated the formulations for *in vitro* release (Table 2). For PmxB, the Gen2 polymers produced significant reductions in burst (from 80% to 35%) as well as sustained release profiles over greater than 24 h (Fig. 3A). We prepared block copolymers containing either PLA or PLGA (50:50 L:G) to evaluate the impact of hydrolytic degradation rate on release, but we observed only minor changes in the release rates between the two polymers [25]. The Lys formulation also exhibited reduced burst from 55% to 40%. Over the first 2–4 h, 80% of Lys release occurred, followed by a transition to a slower release regime over ~200 h (Fig. 3B). This profile was observed for two different classes of PAsp crosslinker: divalent metal cation and polyamine. A lack of effect from the crosslinker suggests the predominance of polymer properties on release kinetics from iFNP NCs.

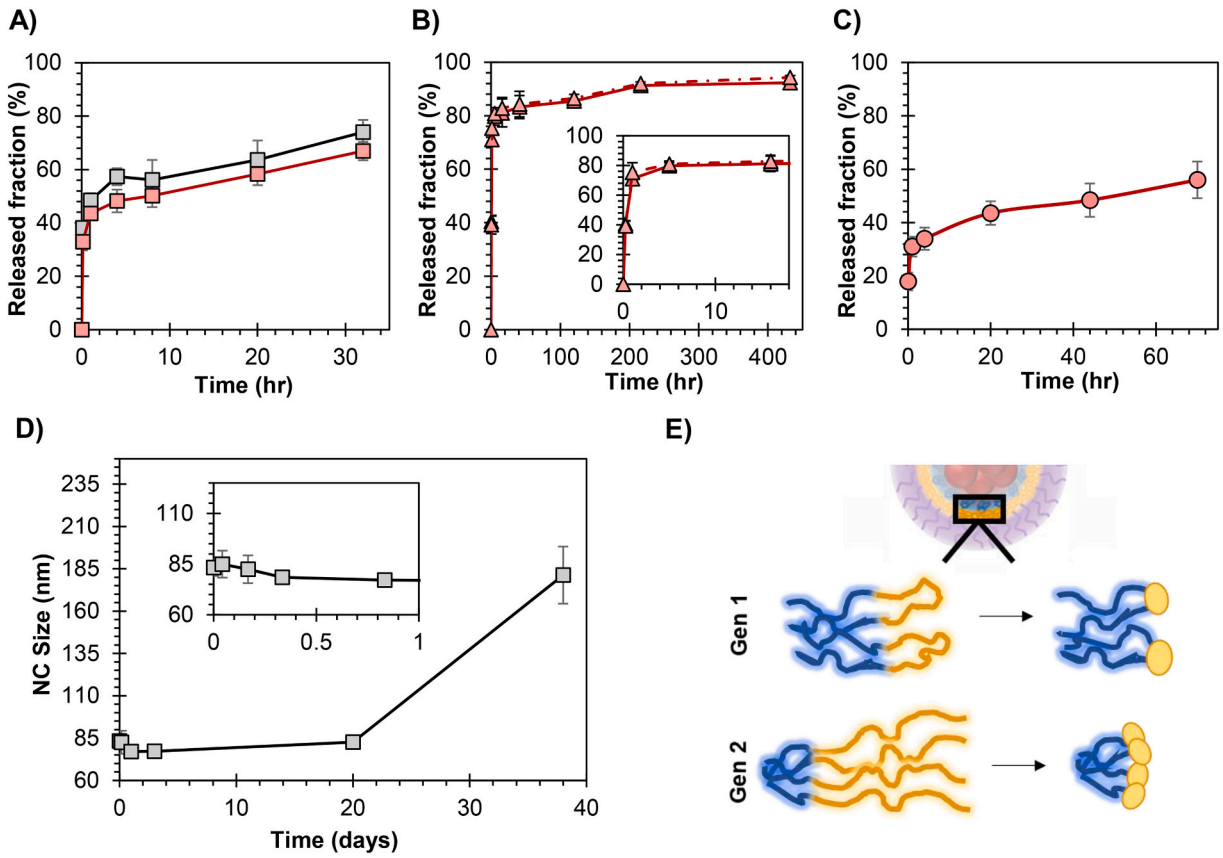

Fig. 3. (A) Release profile of PmxB from NCs formed with Gen2-PLA (red) and Gen2-PLGA (grey). (B) Release profile of Lys from Gen2-PLA NCs and crosslinked with TEPA (solid line) or calcium (dashed line). (C) Release profile of BSA from NCs formed with Gen2-PLA. (D) DLS time course for PmxB NCs stabilized with Gen2-PLGA. Inset is a detail at short times less than 1 day. (E) Schematic illustrating the collapse of PL(*G*)A blocks to form the hydrophobic shell. The relative sizes of the PAsp block (blue) and the PLA block (yellow) dictates the geometric fit upon NC assembly. (For interpretation of the references to colour in this figure legend, the reader is referred to the web version of this article.)

Counterintuitively, the initial release rate of the 14.3 kDa Lys is faster than the much smaller PmxB. This may be due to the higher charge to mass ratio of PmxB, which acts to retain the peptide within the oppositely charged core. An alternative explanation is that Lys preferentially sits at the hydrophobic PLA interface and creates an incomplete PLA shell, which would permit more rapid release of the encapsulated protein after salts in the release media begin to disrupt protein-poly(aspartic acid) interactions. The release profile for BSA, which has a molecular weight 4.5 times larger than Lys and net negative charge, is the slowest of the three model compounds. The overall curve shape is similar across the three species, but BSA exhibits a burst fraction under 20%. These findings indicate that both net charge and molecular weight of the peptide or protein influence release kinetics.

To further understand the impact of the Gen2 polymer on NC size dynamics during *in vitro* release, we monitored formulations by DLS over time. Representative results from PmxB formulated using Gen2-PLGA are shown in Fig. 3D. The inset shows significantly curtailed NC size reduction at short times relative to Gen1-PLA. Colloidal stability was subsequently observed for greater than 20 days. At times longer than a month, significant size growth was observed, but the zeta potential remained neutral throughout. Taken together, these results support the design hypothesis that improved geometric fit of the assembled polymer (due to the shorter PAsp block size) would reduce burst release and result in more sustained release kinetics (Fig. 3E). The molecular weight of the PAsp in Gen1 polymers is 5 kDa, compared to 2 kDa in Gen2. Therefore, the internal crosslinked layer in Gen 2 NCs is thinner than for Gen1 NC. However, even this thinner layer is sufficient to counteract the high osmotic pressure of the core, which is the same from both Gen1 and Gen2 NCs. Upon ion exchange, the Gen1 NC has a higher burst and greater decrease in size then the Gen2 NCs. If the retention of core material were only a result of crosslinking that remained after partial ion exchange, then the Gen1 material should have been more stable. However, the observation is that the Gen2 polymer, whose PLA content relative to PAsp was twice that of Gen1, reduces burst and sustains release rates.

3.3. Gen2 polymer stabilizer effects on encapsulation efficiency

We have previously reported encapsulation efficiencies (EE) using the Gen1-20 polymer stabilizer. These values were 80% ± 2% for PmxB and 98% ± 0.4% for Lys [10]. With the Gen2 polymers, PmxB EE values were 71% ± 3%, Lys values were 92% ± 1%, and BSA values were 73% ± 3%. This slight reduction in EE with the new polymer stabilizer reflects a slight decrease in the charged groups on PAsp relative to those on PmxB or Lys. (Positively charged species like PmxB and Lys had anomalously high EE values in our previous report due to favorable charge interactions.) In contrast, we expected that the improved shell formation would result in increased EE for a neutral encapsulant, which lacks the benefit of charge interactions to aid in retention in the core. With Gen1 polymers, the EE for 5 kDa blue dextran was 17% ± 3% [10]. Indeed, we reformulated this compound using Gen2-PLA and found a significant increase in EE to 43% ± 6%, further supporting the formation of an improved PLA shell using the new polymer architecture.

3.4. Stability of PmxB and Lys after release

A successful delivery vehicle must maintain the chemical and physical structure of the encapsulated therapeutic upon release [29]. In our previous report, we demonstrated the stability of PmxB and Lys in the iFNP process when formulated using Gen1 polymers. The activity of the released Lys fraction was 99% ± 7% of unprocessed enzyme while no impurities were observed at initial times for PmxB [10]. To further confirm there were no adverse effects of NC encapsulation, we monitored the purity of PmxB throughout release and found that it is equivalent to the solution stability of PmxB in buffer (SI Fig. S-6). We also assessed Gen2 formulations for purity of the unencapsulated material and the initial released material to confirm the new synthesis did not impact stability (Table S-1). As before, there were no new impurities in the released PmxB.

3.5. Differential effect of lyophilization on PLA and PLGA NCs

We sought to determine the effect of lyophilization on NC size and PmxB release. We hypothesized that the rehydration of the hydrophilic core could produce release profiles different from those observed with direct transfer of NCs into the release buffer after formation and purification. Inclusion of cryoprotectants trehalose and (2-Hydroxypropyl)-β-cyclodextrin (HPβCD) enabled NC freeze-drying and reconstitution with minimal size change (Fig. 4A). TEM characterization showed spherical particles in good size agreement with DLS data (Fig. 4B). Surprisingly, lyophilization resulted in minor slowing of the release kinetics for Gen2-PLA, but an acceleration for the Gen2-PLGA (Fig. 4C). At 32 h of incubation, over 85% of PmxB was released from Gen2-PLGA but only around 55% from Gen2-PLA. These findings suggest an impact from the dehydration/rehydration of the NCs that is not detectable by physical characterization. Further study will be required to elucidate whether the impact is primarily on the PL(G)A shell itself or on the crosslinked core.

3.6. Lung infection model using PmxB iFNP NCs

We evaluated the Gen2-NC formulations of PmxB in a murine lung infection model using *A. baumannii* [30]. PmxB is typically a last-line agent for multi-drug resistant infections by *A. baumannii*, but toxicity concerns have limited its use more broadly [31,32]. A sustained-release PEG-coated formulation of PmxB would provide two benefits: (1) reduce systemic antibiotic levels while maintaining sufficiently high local concentrations, and (2) enhance mucus diffusion while reducing its binding to mucin [33,34]. In this study, we monitored the infection burden (colony forming units, CFU) at 24 h after treatment, but we did not assess plasma concentration pharmacokinetics. Fig. 5 summarizes bacterial burden for the untreated control, soluble PmxB, and Gen2-NC formulations at a dose of 5 mg/kg PmxB. Gen2-NC formulations dosed at 10 mg/kg, the maximum tolerated dose (MTD) for pulmonary delivery, are tabulated in SI Fig. S-7 along with an additional vehicle control. *Post*

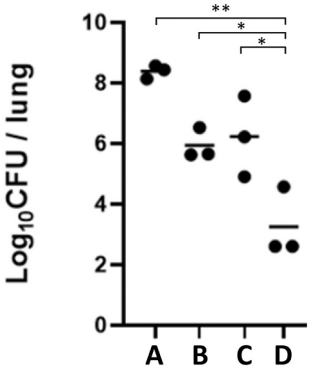

Fig. 5. Lung infection burden 24 h after treatment. Bar indicates average of three animals. (A: no treatment control. B: soluble PmxB at 5 mg/kg. C: Gen2-PLGA at 5 mg/kg. D: Gen2-PLA at 5 mg/kg.) $*p < 0.05$, $**p < 0.001$.

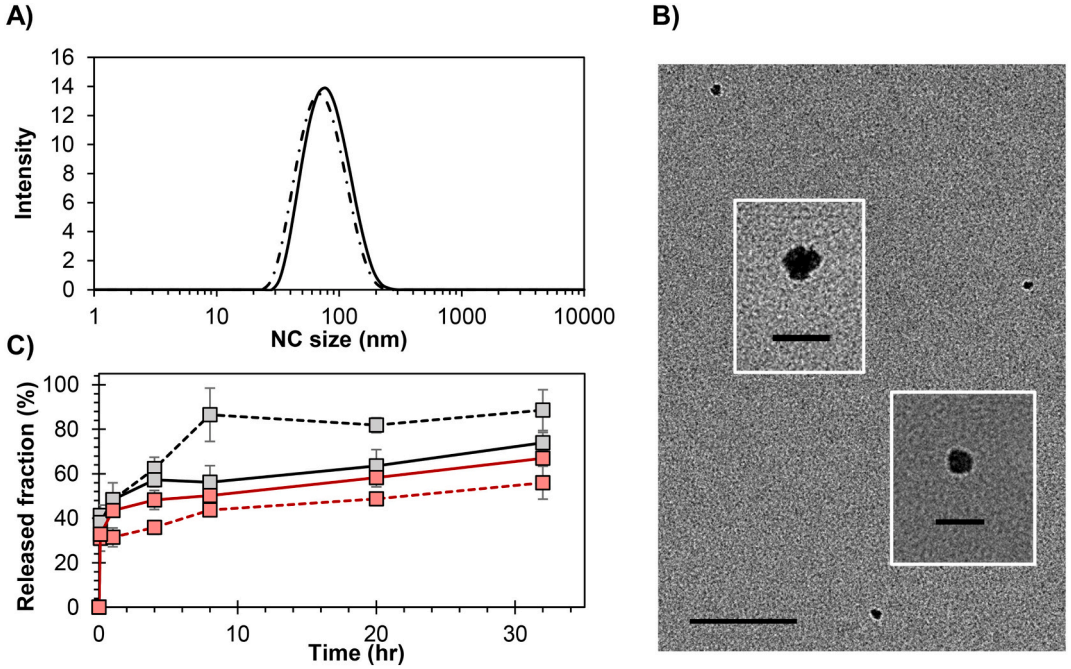

Fig. 4. (A) DLS size distribution for Gen2-PLA NCs encapsulated PmxB before (solid line) and after (dashed line) lyophilization. (B) TEM analysis of the same formulation. Scale bar is 200 nm and the insets are 50 nm. (C) Release profiles for Gen2-PLA (red trace) and Gen2-PLGA (black trace) before (solid) and after (dashed) lyophilization. The solid traces are replicated from Fig. 3 for clarity. (For interpretation of the references to colour in this figure legend, the reader is referred to the web version of this article.)

hoc analysis with Tukey correction was conducted once for the full set of treatment conditions (SI Table S-2). These *p*-values were used for both Fig. 5 and Fig. S-7.

As expected, the bacterial load was highest in the untreated control (Fig. 5 – group A). All treatment arms were better than the untreated control, but only the bacterial reductions from Gen2-PLA (5 mg/kg), Gen2-PLA (10 mg/kg), and Gen2-PLGA (10 mg/kg) were statistically significant (SI Table S-2). Additionally, the Gen2-PLA formulation at 5 mg/kg resulted in significantly lower CFU/lung (2.7-$\log_{10}$ reduction in bacterial burden) than soluble PmxB or Gen2-PLGA at the same dose ($p < 0.05$). We also confirmed that the NC cryoprotectant had no impact on the efficacy of soluble PmxB (SI Fig. S-7). These results demonstrate the release of therapeutically active antibiotic peptide from iFNP formulations after processing. The faster release profiles observed for Gen2-PLGA *in vitro* suggested that it would outperform Gen2-PLA, but this was not observed *in vivo*. It is possible that the Gen2-PLA formulation was more mucodiffusive than the comparable Gen2-PLGA formulation, but this would require further study. Alternatively, the *in vitro* release conditions may not capture all aspects of the *in vivo* lung environment impacting release kinetics. We also dosed Gen2-PLA and Gen2-PLGA at 10 mg/kg, which is the maximum tolerated pulmonary dose [35]. Both formulations resulted in no obvious adverse reactions, likely due to the sustained release design of the formulation. These formulations also effectively reduced bacterial burden (SI Fig. S-7).

3.7. Application of iFNP to delivery challenges

The physical properties of peptide and protein therapeutics limit their transport across biological barriers, including the cell membrane. The present *in vivo* evaluation does not directly probe the question of intracellular delivery. With appropriate surface properties, polymeric carriers such as those produced by iFNP may enable uptake and endosomal escape. This would expand the range of addressable disease targets to include currently undruggable intracellular pathways that are not suitable to small molecule therapeutics. The sequential assembly steps of iFNP permit tuning of the external surface properties of the NC, including the installation of ligands and non-PEG stabilizing brushes. Future work will address the disposition of iFNP-NCs *in vivo* and elucidate these cell interactions.

4. Conclusions

There are few broadly applicable approaches to encapsulating biologics in nanocarriers for sustained release and targeted delivery. We have recently described the inverse Flash NanoPrecipitation (iFNP) process to produce water-dispersible NCs containing peptides, proteins, and RNA. Here we present data on the role of the block copolymer stabilizer in the control of release. We show that the stabilizing polymer characteristics (relative block size, L:G ratio) are dominant factors in tuning release profiles for these NCs. Our findings informed polymer modifications that resulted in sustained release profiles for three model encapsulants. In both cases, the timescale for release was faster than that of polymer degradation (which occurs over the course of about one month). This is consistent with a pore-formation mechanism analogous to that postulated by Discher for polymersomes. The thin PLA shell exaggerates pore opening dynamics due to surface tension effects. Thus, polymer T_g also is a primary contributor to release profiles. Based on these findings, we designed formulations of polymyxin B encapsulated by iFNP that produced release profiles over greater than 24 h. We demonstrated therapeutic efficacy and improved safety profile of these formulations in a gram-negative bacterial lung infection model. These results illustrate the promise that iFNP holds as a new formulation strategy for biologics delivery.

Acknowledgements and funding

This work was supported by the PhRMA Foundation Predoctoral Fellowship in Pharmaceutics (CEM). CEM was also funded by a grant from Optimeos Life Sciences. RKP has a financial interest in Optimeos Life Sciences. J.L. is an Australian National Health and Medical Research Council (NHMRC) Principal Research Fellow.

Appendix A. Supplementary data

Supplementary data to this article can be found online at https://doi.org/10.1016/j.jconrel.2021.04.002.

References

[1] S. Mitragotri, P.A. Burke, R. Langer, Overcoming the challenges in administering biopharmaceuticals: formulation and delivery strategies, Nat. Rev. Drug Discov. 13 (2014) 655–672, https://doi.org/10.1038/nrd4363.
[2] N. Teekamp, L.F. Duque, H.W. Frijlink, W.L.J. Hinrichs, P. Olinga, Production methods and stabilization strategies for polymer-based nanoparticles and microparticles for parenteral delivery of peptides and proteins, Expert Opin. Drug Deliv. 12 (2015) 1311–1331, https://doi.org/10.1517/17425247.2015.1003807.
[3] M. Yu, J. Wu, J. Shi, O.C. Farokhzad, Nanotechnology for protein delivery: overview and perspectives, J. Control. Release 240 (2016) 24–37, https://doi.org/10.1016/j.jconrel.2015.10.012.
[4] A. Akinc, et al., The Onpattro story and the clinical translation of nanomedicines containing nucleic acid-based drugs, Nat. Nanotechnol. 14 (2019) 1084–1087, https://doi.org/10.1038/s41565-019-0591-y.
[5] U. Bulbake, S. Doppalapudi, N. Kommineni, W. Khan, Liposomal formulations in clinical use: an updated review, Pharmaceutics 9 (2) (2017) 12, https://doi.org/10.3390/pharmaceutics9020012. Published 2017 Mar 27.
[6] R. Zaman, et al., Current strategies in extending half-lives of therapeutic proteins, J. Control. Release 301 (2019) 176–189, https://doi.org/10.1016/j.jconrel.2019.02.016.
[7] R.F. Pagels, Polymeric Nanoparticles and Microparticles for the Delivery of Hydrophobic and Hydrophilic Therapeutics, Doctor of Philosophy thesis, Princeton University, 2018.
[8] H. Zhao, et al., Polymer-based nanoparticles for protein delivery: design, strategies and applications, J. Mater. Chem. B 4 (2016) 4060–4071, https://doi.org/10.1039/C6TB00308G.
[9] M. Ye, S. Kim, K. Park, Issues in long-term protein delivery using biodegradable microparticles, J. Control. Release 146 (2010) 241–260, https://doi.org/10.1016/j.jconrel.2010.05.011.
[10] C.E. Markwalter, et al., Polymeric nanocarrier formulations of biologics using inverse Flash NanoPrecipitation, AAPS J. 22 (18) (2020), https://doi.org/10.1208/s12248-019-0405-z.
[11] R.F. Pagels, R.K. Prud'homme, Polymeric nanoparticles and microparticles for the delivery of peptides, biologics, and soluble therapeutics, J. Control. Release 219 (2015) 519–535, https://doi.org/10.1016/j.jconrel.2015.09.001.
[12] S.M. D'Addio, R.K. Prud'homme, Controlling drug nanoparticle formation by rapid precipitation, Adv. Drug Deliv. Rev. 63 (2011) 417–426, https://doi.org/10.1016/j.addr.2011.04.005.
[13] C.E. Markwalter, R.K. Prud'homme, Design of a small-scale multi-inlet vortex mixer for scalable nanoparticle production and application to the encapsulation of biologics by inverse flash nanoprecipitation, J. Pharm. Sci. 107 (2018) 2465–2471, https://doi.org/10.1016/j.xphs.2018.05.003.
[14] W.S. Saad, R.K. Prud'homme, Principles of nanoparticle formation by flash nanoprecipitation, Nano Today 11 (2016) 212–227, https://doi.org/10.1016/j.nantod.2016.04.006.
[15] R.F. Pagels, R.K. Prud'homme, Control of Amphiphile Self-Assembling at the Molecular Level: Supra-Molecular Assemblies with Tuned Physicochemical Properties for Delivery Applications, in: ACS Symposium Series Ch. 11, 1271, American Chemical Society, 2017, pp. 249–274.
[16] B.M. Discher, et al., Polymersomes: tough vesicles made from diblock copolymers, Science 284 (5417) (1999) 1143–1146, https://doi.org/10.1126/science.284.5417.1143.
[17] F. Ahmed, D.E. Discher, Self-porating polymersomes of PEG-PLA and PEG-PCL: hydrolysis-triggered controlled release vesicles, J. Control. Release 96 (2004) 37–53, https://doi.org/10.1016/j.jconrel.2003.12.021.
[18] J.S. Sharp, J.A. Forrest, R.A.L. Jones, Swelling of poly(DL-lactide) and polylactide-co-glycolide in humid environments, Macromolecules 34 (2001) 8752–8760, https://doi.org/10.1021/ma011163q.
[19] O. Vyavahare, D. Ng, S.L. Hsu, Analysis of structural rearrangements of poly(lactic acid) in the presence of water, J. Phys. Chem. B 118 (2014) 4185–4193, https://doi.org/10.1021/jp500219j.
[20] S.-E. Cheah, et al., New pharmacokinetic/pharmacodynamic studies of systemically administered colistin against *Pseudomonas aeruginosa* and *Acinetobacter baumannii* in mouse thigh and lung infection models: smaller

response in lung infection, J. Antimicrob. Chemother. 70 (2015) 3291–3297, https://doi.org/10.1093/jac/dkv267.
[21] R.V. Dudhani, J.D. Turnidge, R.L. Nation, J. Li, fAUC/MIC is the most predictive pharmacokinetic/pharmacodynamic index of colistin against *Acinetobacter baumannii* in murine thigh and lung infection models, J. Antimicrob. Chemother. 65 (2010) 1984–1990, https://doi.org/10.1093/jac/dkq226.
[22] R.V. Dudhani, et al., Elucidation of the pharmacokinetic/pharmacodynamic determinant of colistin activity against *Pseudomonas aeruginosa* in murine thigh and lung infection models, Antimicrob. Agents Chemother. 54 (2010) 1117, https://doi.org/10.1128/AAC.01114-09.
[23] Institute, C. a. L. S, Vol. M100Ed30, 2020.
[24] R.A. Miller, J.M. Brady, D.E. Cutright, Degradation rates of oral resorbable implants (polylactates and polyglycolates): rate modification with changes in PLA/PGA copolymer ratios, J. Biomed. Mater. Res. 11 (1977) 711–719, https://doi.org/10.1002/jbm.820110507.
[25] H.K. Makadia, S.J. Siegel, Poly lactic-co-glycolic acid (PLGA) as biodegradable controlled drug delivery carrier, Polymers 3 (2011) 1377–1397, https://doi.org/10.3390/polym3031377.
[26] L. Lu, et al., In vitro and in vivo degradation of porous poly(DL-lactic-co-glycolic acid) foams, Biomaterials 21 (2000) 1837–1845, https://doi.org/10.1016/S0142-9612(00)00047-8.
[27] B.W. McCarty, E.T. Adams, Osmotic pressure measurements of ovalbumin and lysozyme mixtures, Biophys. Chem. 28 (1987) 149–159, https://doi.org/10.1016/0301-4622(87)80084-4.
[28] Y.U. Moon, C.O. Anderson, H.W. Blanch, J.M. Prausnitz, Osmotic pressures and second virial coefficients for aqueous saline solutions of lysozyme, Fluid Phase Equilib. 168 (2000) 229–239, https://doi.org/10.1016/S0378-3812(99)00337-4.
[29] M.C. Manning, D.K. Chou, B.M. Murphy, R.W. Payne, D.S. Katayama, Stability of protein pharmaceuticals: an update, Pharm. Res. 27 (2010) 544–575, https://doi.org/10.1007/s11095-009-0045-6.
[30] M. Alsan, M. Klompas, *Acinetobacter baumannii*: an emerging and important pathogen, J. Clin. Outcomes Manag. 17 (2010) 363–369.
[31] A.P. Zavascki, L.Z. Goldani, J. Li, R.L. Nation, Polymyxin B for the treatment of multidrug-resistant pathogens: a critical review, J. Antimicrob. Chemother. 60 (2007) 1206–1215, https://doi.org/10.1093/jac/dkm357.
[32] M.U. Ahmed, et al., Potential toxicity of polymyxins in human lung epithelial cells, Antimicrob. Agents Chemother. 61 (2017) 1–12, https://doi.org/10.1128/AAC.02690-16.
[33] Q. Xu, et al., Impact of surface polyethylene glycol (PEG) density on biodegradable nanoparticle transport in mucus ex vivo and distribution in vivo, ACS Nano 9 (2015) 9217–9227.
[34] J.X. Huang, et al., Mucin binding reduces colistin antimicrobial activity, Antimicrob. Agents Chemother. 59 (2015) 5925–5931, https://doi.org/10.1128/AAC.00808-15.
[35] Y.-W. Lin, et al., Aerosolized polymyxin B for treatment of respiratory tract infections: determination of pharmacokinetic-pharmacodynamic indices for aerosolized polymyxin B against *Pseudomonas aeruginosa* in a mouse lung infection model, Antimicrob. Agents Chemother. 61 (2017) e00211–e00217, https://doi.org/10.1128/AAC.00211-17.